

**Copper (I) sulfide: A two-dimensional semiconductor with superior oxidation resistance and high carrier mobility**

Journal:	<i>Nanoscale Horizons</i>
Manuscript ID	NH-COM-08-2018-000216.R1
Article Type:	Communication
Date Submitted by the Author:	17-Sep-2018
Complete List of Authors:	Guo, Yu; Dalian University of Technology, Physics Wu, Qisheng; Southeast University, Physics; University of Nebraska-Lincoln, Chemistry Li, Yunhai; Southeast University, Physics Lu, Ning; Anhui Normal University, Mao, Keke; University of Science and Technology of China, Bai, Yizhen; Dalian University of Technology, School of Physics Zhao, Jijun; Dalian University of Technology Wang, Jinlan; Southeast University, Department of Physics Zeng, Xiao Cheng; University of Nebraska-Lincoln, Department of Chemistry

Conceptual insights

Copper sulfides have been extensively studied owing to their high abundance, easy preparation, and outstanding chemical and physical properties. Here we report a *hitherto* unreported 2D copper (I) sulfide, namely, δ -Cu₂S monolayer. δ -Cu₂S monolayer is a semiconductor with a desirable direct band gap of 1.26 eV, close to that of bulk silicon, as well as a high electron mobility up to 6880 cm²V⁻¹s⁻¹, about 27 times of that of the β -Cu₂S bilayer (246 cm²V⁻¹s⁻¹, measured value). Unlike many other 2D modest-band-gap semiconductors which have relatively low chemical stability, notably, the δ -Cu₂S monolayer exhibits superior oxidation resistance, as demonstrated by the high activation energy of 1.98 eV for the chemisorption of O₂ on δ -Cu₂S. Another novel feature of the δ -Cu₂S solid is that it has much lower formation energy compared with the previous known β -Cu₂S solid, suggesting high likelihood of achieving δ -Cu₂S monolayer in the laboratory.

Copper (I) sulfide: A two-dimensional semiconductor with superior oxidation resistance and high carrier mobility

Yu Guo,^{ab} Qisheng Wu,^{bc} Yunhai Li,^c Ning Lu,^d Keke Mao,^{be} Yizhen Bai,^a Jijun Zhao,^{*a} Jinlan Wang^{*cf} and Xiao Cheng Zeng ^{*bg}

^aKey Laboratory of Materials Modification by Laser, Ion and Electron Beams (Dalian University of Technology), Ministry of Education, Dalian, Liaoning 116024, China

^bDepartment of Chemistry, University of Nebraska–Lincoln, Lincoln, Nebraska 68588, United States

^cSchool of Physics, Southeast University, Nanjing, Jiangsu 211189, China

^dAnhui Province Key Laboratory of Optoelectric Materials Science and Technology, Department of Physics, Anhui Normal University, Wuhu, Anhui 241000, China

^eSchool of Energy and Environment Science, Anhui University of Technology, Maanshan, Anhui 243032, China

^fSynergetic Innovation Center for Quantum Effects and Applications (SICQEA), Hunan Normal University, Changsha, Hunan 410081, China

^gDepartment of Chemical & Biomolecular Engineering and Department of Mechanical & Materials Engineering, University of Nebraska–Lincoln, Lincoln, Nebraska 68588, United States

Y.G. and Q.W. contributed equally to this work

Abstract

Two-dimensional (2D) semiconductor with suitable direct band gap, high carrier mobility, and excellent open-air stability is especially desirable for material applications. Herein, we show theoretical evidence of a new phase of copper (I) sulfide (Cu₂S) monolayer, named as δ -Cu₂S, with both novel electronic properties and superior oxidation resistance. We find that both monolayer and bilayer δ -Cu₂S have much lower formation energy compared with the known β -Cu₂S phase. Given that the β -Cu₂S sheets have been recently synthesized in the laboratory (*Adv. Mater.* **2016**, 28, 8271), the higher stability of δ -Cu₂S over β -Cu₂S sheets suggests high possibility of experimental realization of δ -Cu₂S. Stability analysis indicates that δ -Cu₂S is dynamically and thermally stable. Notably, δ -Cu₂S exhibits superior oxidation resistance, due to the high activation energy of 1.98 eV for the chemisorption of O₂ on δ -Cu₂S. On electronic

*Corresponding authors: zhaojj@dlut.edu.cn (J. Zhao); jlwang@seu.edu.cn (J. Wang); xzeng1@unl.edu (X. C. Zeng)

properties, δ -Cu₂S is a semiconductor with a modest direct band gap (1.26 eV) and an ultrahigh electron mobility up to 6880 cm²V⁻¹s⁻¹, about 27 times of that (246 cm²V⁻¹s⁻¹) for the β -Cu₂S bilayer. The marked difference between electron and hole mobility of δ -Cu₂S suggests easy separation of electrons and holes for solar energy conversion. Combination of these novel properties renders δ -Cu₂S a promising 2D material for future applications in electronics and optoelectronics with high thermal and chemical stability.

Conceptual insights

Copper sulfides have been extensively studied owing to their high abundancy, easy preparation, and outstanding chemical and physical properties. Here we report a *hitherto* unreported 2D copper (I) sulfide, namely, δ -Cu₂S monolayer. δ -Cu₂S monolayer is a semiconductor with a desirable direct band gap of 1.26 eV, close to that of bulk silicon, as well as a high electron mobility up to 6880 cm²V⁻¹s⁻¹, about 27 times of that of the β -Cu₂S bilayer (246 cm²V⁻¹s⁻¹, measured value). Unlike many other 2D modest-band-gap semiconductors which have relatively low chemical stability, notably, the δ -Cu₂S monolayer exhibits superior oxidation resistance, as demonstrated by the high activation energy of 1.98 eV for the chemisorption of O₂ on δ -Cu₂S. Another novel feature of the δ -Cu₂S solid is that it has much lower formation energy compared with the previous known β -Cu₂S solid, suggesting high likelihood of achieving δ -Cu₂S monolayer in the laboratory.

Introduction

Copper sulfide (Cu_{2-x}S , $0 \leq x \leq 1$) nanomaterials have been extensively studied owing to their high abundance, easy preparation, and excellent chemical and physical properties.¹⁻⁴ In the laboratory, Cu_{2-x}S can be synthesized using various methods, e.g., the colloidal solution process, the wet chemical method, and the facile solvothermal method.⁵⁻⁸ Among many Cu_{2-x}S nanomaterials, Cu_2S (chalcocite) is known for its excellent optical and electronic properties with potential applications in lithium storage,⁹ high-capacity cathode materials in lithium secondary batteries,¹⁰ photocatalysts,¹¹ and absorber in photovoltaic conversions.¹²⁻¹⁴ Bulk Cu_2S solids are usually classified as α phase (stable above 425 °C), β phase (high chalcocite; stable between 105 and 425 °C) and γ phase (low chalcocite; the first solid-liquid hybrid phase, and stable below 105 °C),¹⁵ respectively. Phase transition between the high and low chalcocite phases could be achieved by heating with the electron beam at relatively low temperature.^{5, 16, 17}

Two-dimensional (2D) materials have attracted extensive attentions due largely to many of their novel properties are not seen in the bulk counterparts.¹⁸⁻²³ Very recently, 2D β - Cu_2S sheets with the thickness down to 1.8 nm have been synthesized and proven to exist as a hybrid solid-liquid phase.^{8, 24, 25} The temperature (−15 °C) for high chalcocite to low chalcocite transition is much lower than that of the bulk counterpart (105 °C), rendering 2D β - Cu_2S sheet available for room-temperature applications.⁸ Similarly, the transition temperature from β - Cu_2S to γ - Cu_2S also decreases with decreasing nanoparticle size.²⁶ In addition, Cu_2S sheet exhibits higher photoactivity for solar energy conversion than its bulk counterpart.²⁷ A previous theoretical calculation predicted that β - Cu_2S bilayer is the thinnest stable layer as the two layers are strongly bonded, evidenced by the large binding energy between layers (0.93 eV per Cu_2S unit).²⁴ Moreover, β -

Cu₂S bilayer exhibits a direct band gap of 0.9 eV at the high-symmetry point Γ ,⁸ implying that β -Cu₂S bilayer could be a promising candidate for electronic and optical applications.

Although the solid-liquid phase is quite interesting,^{8, 15, 24} it also indicates meta-stability and rapid diffusion of atoms, which may degrade the materials performance. In this article, we predict a new phase of Cu₂S monolayer, named as δ -Cu₂S, based on global structural search and first-principles calculations. Our computation indicates that δ -Cu₂S monolayer and bilayer are semiconductors with modest direct band gap and ultrahigh electron mobility up to 6880 cm²V⁻¹s⁻¹ and 5786 cm²V⁻¹s⁻¹, respectively. The latter is more than one order of magnitude higher than that of bilayer β phase (246 cm²V⁻¹s⁻¹). Our computation also shows that δ -Cu₂S is dynamically and thermally stable, and chemically inert upon oxidation. In particular, the superior oxidation resistance of the δ -Cu₂S, due to high activation energy (1.98 eV) for the chemisorption of O₂ on this 2D sheet, is the distinct feature compared with many ultrathin 2D materials with poor chemical stability in open air.²⁸⁻³¹ A well-known example is the black phosphorus whose 2D counterpart - phosphorene - is hydrophilic and can be easily oxidized in the air moisture with a low activation energy of 0.70 eV.³² Oxidation of phosphorene leads to higher contact resistance, lower carrier mobility, and possible mechanical degradation and breakdown.^{29, 32, 33}

Results and Discussions

After the systematic structural search, hundreds of structures are generated by using the CALYPSO code. Four representative low-lying structures are shown in Electronic Supplementary Information (ESI) Fig. S1, and their stability analyses are presented in ESI Fig. S2 and Table S1. The δ -Cu₂S monolayer is identified as the most stable 2D structure. Fig. 1a presents the optimized structure of δ -Cu₂S, with the tetragonal structure and lateral isotropy. The

unit cell of δ -Cu₂S has four Cu and two S atoms, with each Cu atom being bonded with five Cu atoms and two S atoms, and each S atom being bonded with four Cu atoms. As shown in Fig. 1a, the optimized 2D layered structure has a lattice constant (a) of 5.02 Å and a thickness (h) of 2.55 Å along z direction, with average Cu-S and Cu-Cu bond lengths of 2.22 Å and 2.57 Å, respectively (see Table 1). To gain insight into the chemical bond of δ -Cu₂S, we calculate the electron localization function (ELF).³⁴⁻³⁶ As displayed in Fig. 1b, the electrons are mainly localized around S atoms and absent in the middle region between Cu and S atoms, indicating distinct feature of ionic bonding. In addition, Bader charge analysis^{37, 38} shows substantial amount of electrons, i.e., 0.32 e donated from each Cu atom to S atoms (Table 1).

Table 1. Lattice constant (a), bond lengths of Cu-Cu (l_1) and Cu-S (l_2), the angle (θ) of Cu-S-Cu, and thickness (h) of δ -Cu₂S as shown in Fig. 1(a); Bader charge (Q_{Cu}) transferred from each Cu atom to S atom; effective masses (m) of carriers, deformation potential constants (E_1), elastic modulus (C_{2D}) and carrier mobility (μ) for δ -Cu₂S monolayer (δ -monolayer), δ -Cu₂S bilayer (δ -bilayer), β -Cu₂S bilayer (β -bilayer) along armchair and zigzag directions.

a (Å)	l_1 (Å)	l_2 (Å)	θ (°)	h (Å)	Q_{Cu} (e)
5.02	2.57	2.22	70.76	2.55	0.32
Material	Carrier type	m (m_0)	E_1 (eV)	C (J•m ⁻²)	μ (cm ² V ⁻¹ s ⁻¹)
δ -monolayer	hole	4.28	1.79	40.59	14.54
	electron	0.21	1.71	40.59	6880.17
δ -bilayer	hole	0.23	4.28	94.99	2107.74
	electron	0.16	3.66	94.99	5786.28
β -bilayer (armchair)	hole	0.98	4.79	63.99	79.68
	electron	0.49	5.07	63.99	222.09
β -bilayer (zigzag)	hole	0.59	5.00	65.78	109.37
	electron	0.47	5.35	65.78	246.51

To evaluate the energetic stability of δ -Cu₂S, we first calculate the formation energy ΔH defined as

$$\Delta H = \frac{E_{\text{tot}} - n_1 \times E_{\text{Cu}} - n_2 \times E_{\text{S}}}{n} \quad (1)$$

where E_{tot} is the total energy of δ -Cu₂S, E_{Cu} and E_{S} are the energy per atom of a body-centered cubic (bcc) Cu and a orthorhombic S₁₂₈ solids, respectively. The factors n_1 and n_2 denote the number of Cu atoms and S atoms, while the factor n represents the total number of atoms in the unit cell. The calculated ΔH is -0.21 eV/atom, revealing that formation of δ -Cu₂S is exothermic. Remarkably, this value is far lower than that of the β -Cu₂S ($\Delta H = -0.01$ eV/atom) shown in Fig. S1, implying high possibility to synthesize δ -Cu₂S in the laboratory.

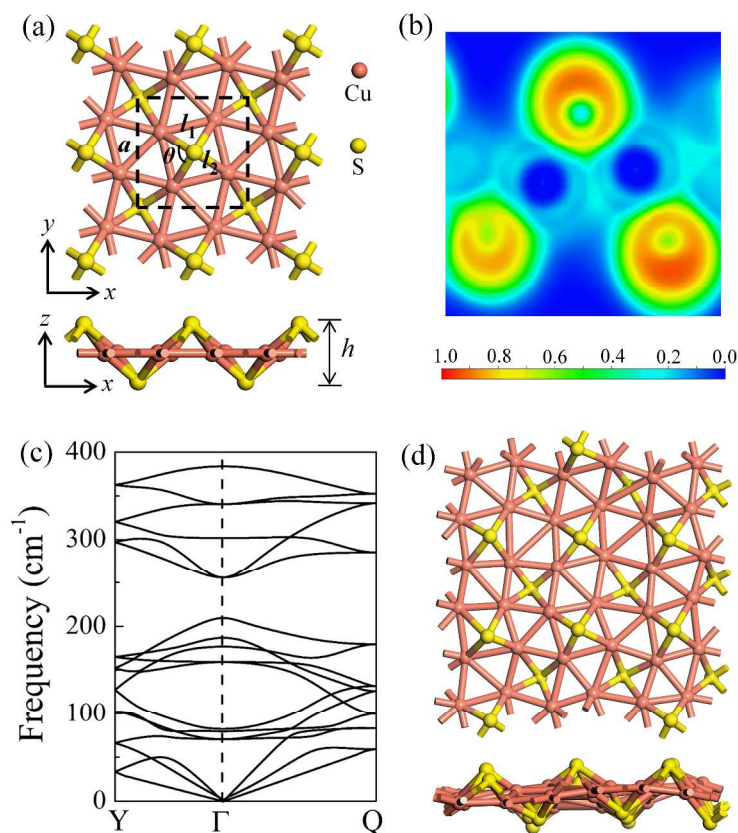


Fig. 1. (a) The atomic structure of δ -Cu₂S from top view and side views, respectively. The unit cell is denoted by dashed lines. a , l_1 , l_2 , θ and h represent the lattice constant, bond lengths of Cu-

Cu and Cu-S, the bond angle of Cu-S-Cu, the layer thickness along z direction, respectively. (b) Electron localization function (ELF); ELF = 1 (red) and 0 (blue) indicate accumulated and vanishing electron density, respectively. (c) Phonon dispersion of δ -Cu₂S. High-symmetry points of the first Brillouin zone are Y (0, 0.5, 0), Γ (0, 0, 0) and Q (0.5, 0.5, 0), as shown in Fig. 4b. (d) Snapshots of the equilibrium structures of the Cu₂S monolayer at 800 K after 10 ps *ab initio* molecular dynamic simulation. Cu and S atoms are shown in pink and yellow colors, respectively.

Since the experimentally synthesized δ -Cu₂S sheets could be multilayer rather than monolayer, we also considered several high-symmetry stacking configurations for δ -Cu₂S monolayers. We find that the AA stacking in Fig. 4b is the most stable bilayer configuration with interlayer binding energy of -0.08 eV/atom, comparable with that for graphene and phosphorene (around -0.06 eV/atom) bilayer.^{39,40} According to the Equation (1), the formation energy (-0.13 eV/atom) for δ -Cu₂S bilayer is also much lower than that of β -Cu₂S bilayer, again suggesting likelihood of synthesis of δ -Cu₂S bilayer.

The dynamic stability of δ -Cu₂S is confirmed by the absent of imaginary frequencies in computed phonon dispersion (Fig. 1c). We also performed Born-Oppenheimer molecular dynamics (BOMD) simulations to examine thermal stability of the 2D structure at elevated temperature. The BOMD simulations show that δ -Cu₂S monolayer can maintain its structural integrity even up to 800 K for 10 ps (Fig. 1d), indicating its exceeding stability even above the room temperature. At temperature of 900 K, the planar structure is highly distorted within 10 ps of BOMD simulation (Fig. S4d). Furthermore, for both Cu and S atoms, we calculate the mean-square-diffusion distance,⁸ defined as $S = 1/N \sum_1^N (\Delta x^2 + \Delta y^2 + \Delta z^2)$ where N is the number of atoms for each element, and Δx , Δy and Δz are the differences of Cartesian coordinates for the

same atom at the beginning and ending of the BOMD simulation. As shown in Fig. 2, the mean-square-diffusion distance for Cu and S atoms remain almost unchanged with time t . At temperature of 800 K, the S atoms diffuse a bit more than the Cu atoms since the Cu atoms are covered by the S atoms (see Fig. 1a). The computed time-dependent mean-square-diffusion distance of the Cu and S atoms indicate that the δ -Cu₂S monolayer is still in solid phase at 800 K, contrary to the hybrid solid-liquid phase of bulk β -Cu₂S at room temperature.⁸ This result further supports that δ -Cu₂S monolayer has higher structural stability than β -Cu₂S monolayer at room temperature.

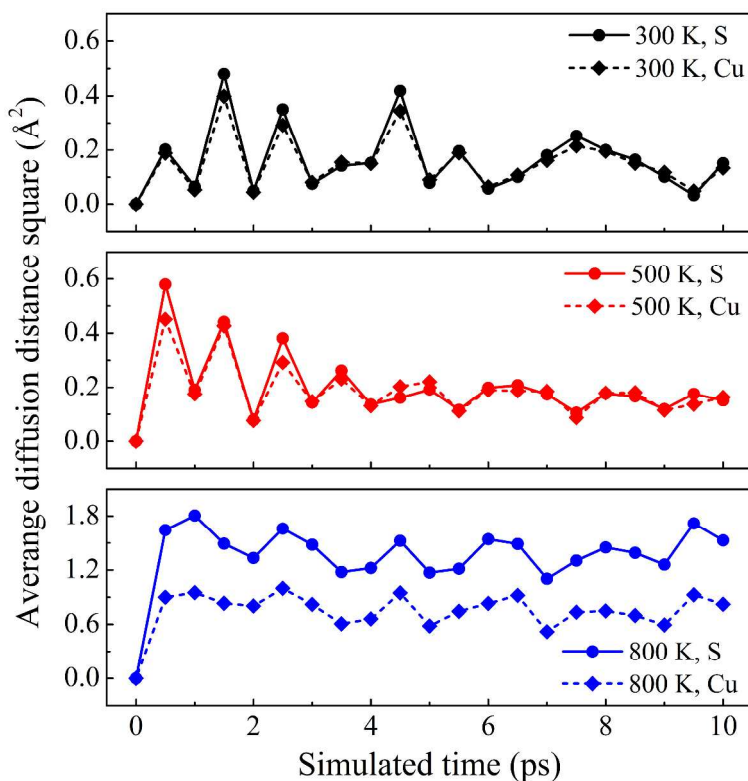


Fig. 2. Average diffusion distance squares as functions of simulated time for δ -Cu₂S at 300 K, 500 K and 800 K from top to bottom panels, respectively.

To examine chemical stability of δ -Cu₂S monolayer in open-air environment, we investigate physisorption and chemisorption of O₂ molecule on the surface of 2D sheet, and compute the

dissociative oxidation pathway. The interaction between O₂ and the monolayer is described by the binding energy (E_{bind}) defined as follows:

$$E_{bind} = E_{tot} - E_{\delta} - E_{O_2} \quad (2)$$

where E_{tot} , E_{δ} , and E_{O_2} are the energies of δ -Cu₂S monolayer with an O₂ molecule adsorbed, δ -Cu₂S monolayer, and a single O₂ molecule in triplet spin state, respectively. By definition, a negative E_{bind} means exothermic adsorption of O₂ molecule.

Fig. 3 illustrates the adsorption configurations and dissociation process for an O₂ molecule, initially physisorbed on the δ -Cu₂S, turning into two oxygen atoms chemisorbed on the monolayer. In the initial stage of physisorption, O₂ molecule is located about 3.7 Å above the surface of δ -Cu₂S with binding energy of -0.09 eV. As the O₂ molecule approaches to the 2D sheet, the O–O bond is elongated to 1.65 Å at the transition state. The O₂ molecule undergoes a transition from physisorption to chemisorption by overcoming an activation energy (E^a) of 1.98 eV, suggesting an extremely slow oxidation rate at room temperature. This activation energy is even greater than that calculated for MoS₂ monolayer (1.59 eV),⁴¹ which already exhibits relatively high resistance to O₂ chemisorption. Thus, δ -Cu₂S monolayer is expected to be a superior oxidation-resistant material, as MoS₂ monolayer. Note that we have considered several other adsorption sites for O₂ and selected the initial and final structures with the lowest binding energy to simulate the oxidation process of δ -Cu₂S (see ESI S4 for details).

The bonding energy of O₂ is often overestimated by DFT/PBE calculations. If we adopt the experimental value of O₂ bonding energy (5.16 eV)⁴² instead of the DFT value, the binding energy (E_{bind}^*) could be redefined as:

$$E_{bind}^* = E_{tot} - E_{\delta} - 2 \times E_O - E_{bond} \quad (3)$$

where E_{tot} , E_{δ} , E_O , E_{bond} are the energies of δ -Cu₂S monolayer adsorbed with an O₂ molecule, pristine δ -Cu₂S monolayer, and an O atom, the experimental O₂ bonding energy, respectively. Based on Eq. (3), the binding energies for initial, transition and final states are -1.74 , 0.24 and -1.82 eV, respectively (see ESI Table S2), which are lower than those based on using calculated O₂ bonding energy as the reference (see Eq. (2)). It indicates that O₂ could bind strongly with δ -Cu₂S monolayer. However, there is no change with the activation energy of 1.98 eV, which is still hard to overcome.

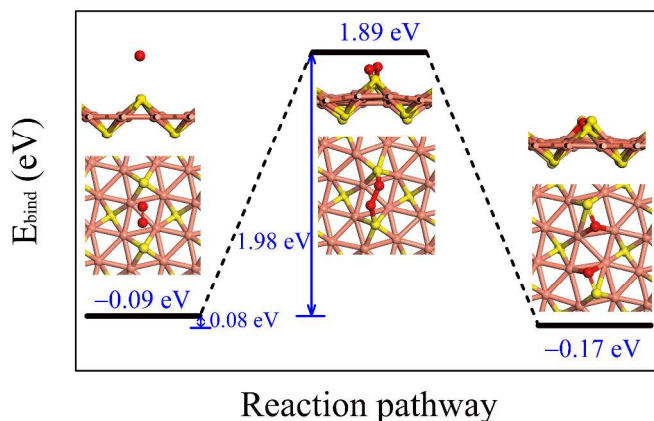


Fig. 3. Reaction pathway for an O₂ molecule to dissociate into two O atoms on the δ -Cu₂S. The black line segments indicate the energy levels of the initial, transition, and final states, respectively, with corresponding atomic structures (top and side views) given next to the energy level. The blue numbers give (from left to right) the binding energy of the initial state, heat of reaction, activation energy, and binding energy of the transition and final states, respectively. The O, S and Cu atoms are painted in red, yellow and pink, respectively.

To characterize the thermal stability of the oxidized products, we define the heat of reaction as follows:

$$E^H = E_{bind}^{phys} - E_{bind}^{chem} \quad (4)$$

where E_{bind}^{phys} and E_{bind}^{chem} are the binding energies for O_2 physisorbed and chemisorbed on the δ - Cu_2S monolayer at the corresponding equilibrium state, respectively. As displayed in Fig. 3, E^H obtained for δ - Cu_2S is as low as 0.08 eV, demonstrating weak driving force for an O_2 molecule to dissociate, and to be chemisorbed on the 2D sheet, suggesting again high resistivity to oxidation and superior chemical inertness in ambient air. Thus, δ - Cu_2S monolayer could offer long-term stability and durability for sustained device performance. To gain additional insight into good chemical stability against O_2 oxidation, we performed BOMD simulation of δ - Cu_2S monolayer exposed to gas-phase O_2 at room temperature (ESI S6). Here, six O_2 molecules (per supercell) are initially placed about 4 Å above the surface of δ - Cu_2S monolayer. The 5-ps simulation indicates that O_2 molecules tend to either bounce back or move away from the surface, rather than dissociate into oxygen atoms (ESI Movie S1). This simulation suggests good stability of δ - Cu_2S monolayer against O_2 oxidization.

The electronic band structure and local density of states (LDOS) of δ - Cu_2S monolayer are computed by using the HSE06 functional (Fig. 4a). The HSE06 computation suggests that δ - Cu_2S possesses a modest direct band gap of 1.26 eV at Γ point, 0.24 eV smaller than the HSE06 bandgap of 1.50 eV for bilayer β - Cu_2S (ESI Fig. S3). The LDOS analysis reveals that the edges of the valence bands are dominated by the $3d$ orbitals of Cu atoms, while the conduction band edges stem mainly from the $3d$ orbitals of Cu atoms and partially from the $3p$ orbitals of S atoms. Hence, Cu atoms make the major contribution to both the valence band maximum (VBM) and the conduction band minimum (CBM). Meanwhile, the substantial overlap of the LDOS near the Fermi level implies strong hybridization between the orbitals of Cu and S atoms. The computed carrier effective masses are $4.28 m_0$ for holes and $0.21 m_0$ for electrons, respectively. The relatively small effective mass for electrons suggests that the carriers are rather mobile in the 2D

sheet. Moreover, the large difference in effective masses can be exploited to separate the electrons and holes for solar energy conversion.

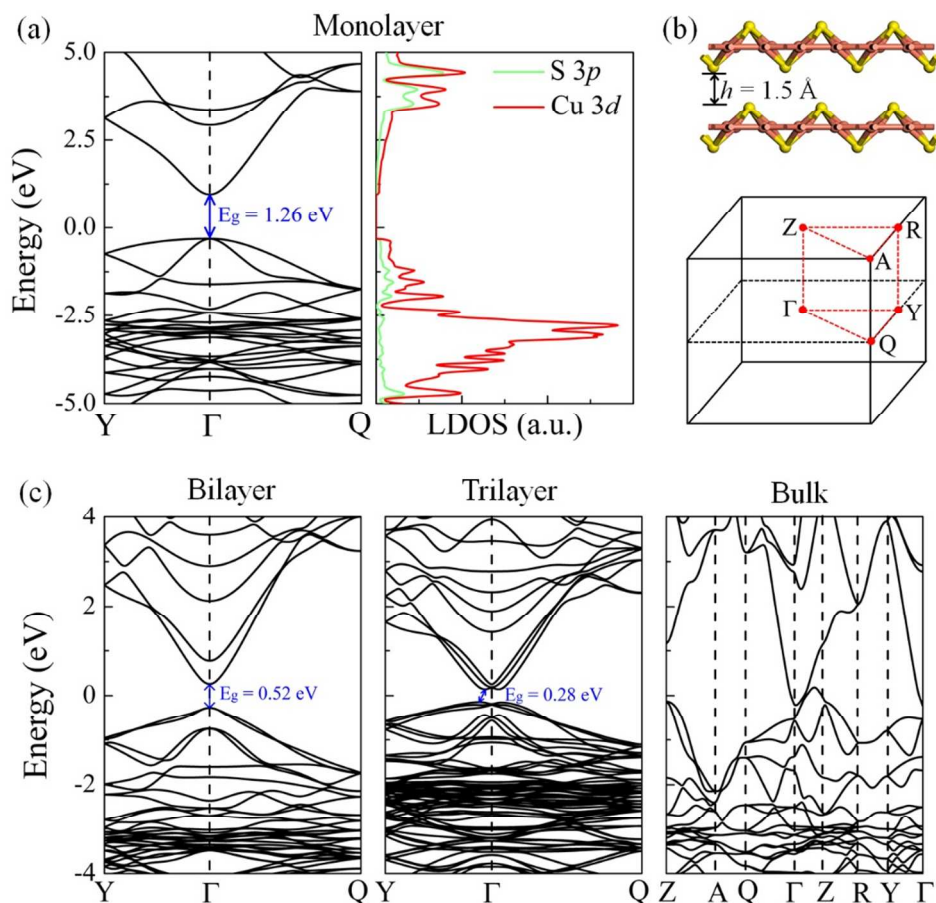


Fig. 4. (a) Electronic band structure (right panel) and local density of states (LDOS, left panel) of monolayer δ -Cu₂S sheet. Green and red lines in LDOS represent contributions from S 3p and Cu 3d states, respectively. (b) Atomic structure of layers of δ -Cu₂S and Brillouin zone of bulk counterpart. (c) Electronic band structures of bilayer, trilayer and bulk δ -Cu₂S, respectively. E_g is the band gap denoted by the solid arrow. The Fermi levels are set to zero.

Strain engineering offers a useful way to tune the electronic properties and performance of 2D atomic crystals. For example, a linear decrease in the optical band gap of MoS₂ with strain has been experimentally confirmed via photoluminescence.^{43, 44} To examine the strain effect on

the band gap of δ -Cu₂S monolayer, we compute the electronic band structures of δ -Cu₂S monolayer under various biaxial strains up to $\pm 3\%$ (see ESI Fig. S7 for details). The results indicate that the band gap of δ -Cu₂S monolayer linearly increases from 1.07 eV to 1.55 eV under the strain of -3% to 3% , which is similar to the strain effect on MoS₂. The direct character and dispersion (see ESI Fig. S7 and S8) are preserved. For the multilayered system, as layer thickness increases, the band gap decreases monotonically. Consequently, δ -Cu₂S bilayer and trilayer preserve the semiconducting behavior, with band gap of 0.52 eV (direct) and 0.28 eV (indirect), while bulk δ -Cu₂S is metallic. Furthermore, δ -Cu₂S bilayer possesses much smaller carrier effective masses of $0.23 m_0$ for holes and $0.16 m_0$ for electrons, compared with those of β -Cu₂S bilayer ($0.56 \sim 0.98 m_0$ for holes and $0.47 \sim 0.49 m_0$ for electrons), as listed in Table 1, implying easy transport of carriers in δ -Cu₂S bilayer.

To further characterize the electron transport properties of δ -Cu₂S monolayer, we calculate their acoustic phonon-limited carrier mobility μ , based on the Takagi model within the deformation potential approximation:⁴⁵⁻⁴⁷

$$\mu = \frac{e\hbar^3 C_{2D}}{k_B T m m_d (E_1)^2} \quad (5)$$

where e is the electron charge, \hbar is the reduced Planck constant, k_B is the Boltzmann constant, T is the temperature, m is the effective mass along the transport direction, $m_d = \sqrt{m m_\perp}$ is the average effective mass (m_\perp is the effective mass perpendicular to the transport direction), C_{2D} is the elastic modulus of the 2D sheet, determined by the lattice parameter l along the transport direction via $\Delta E/S_0 = C_{2D}(\Delta l/l)^2/2$ (ΔE is the energy change of the system under lattice deformation Δl , S_0 is the area of unit cell). The term E_1 represents the deformation potential constant of the VBM for a hole, or the CBM for an electron along the transport direction, defined by $\Delta V/(\Delta l/l)$ (ΔV is the band edge shift under lattice deformation). All data are calculated with

using a strain step of 0.5%. The temperature used in the mobility calculations is 300 K. The present carrier mobility calculation has been demonstrated to be physically reasonable and computationally efficient.⁴⁸⁻⁵⁰

As listed in Table 1, the electron mobility of δ -Cu₂S monolayer can reach as high as 6880 cm²V⁻¹s⁻¹, about five times higher than that of phosphorene (1140 cm²V⁻¹s⁻¹)⁴⁸. The high carrier mobility is attributed to the small effective mass, large elastic modulus, and small deformation potential constant. δ -Cu₂S monolayer shows C_{2D} values up to 40.59 J•m⁻², larger than the value of phosphorene (28.94 J•m⁻² along armchair direction),⁴⁸ resulting in small-amplitude lattice waves and weak scattering with charge carriers. The deformation potential constant E_1 is another important factor for carrier mobility. It approximately describes the strength of electron–phonon coupling and is determined by the band edge shift under lattice variation due to acoustic phonons. Here, E_1 is as low as 1.71 eV, contributing to the ultra-high carrier mobility. The high electron mobility demonstrates that δ -Cu₂S monolayer is a good candidate for 2D electronic devices. Furthermore, the carrier mobility of electron is three orders of magnitude larger than that of hole (14 cm²V⁻¹s⁻¹). The substantial difference between the transport behavior of electrons and holes could be beneficial to controlling the carrier transport, and separating the carriers to promote the device performance. More importantly, the electron mobility of δ -Cu₂S bilayer is as high as 5786 cm²V⁻¹s⁻¹, about 25 times of that of β -Cu₂S bilayer (222 cm²V⁻¹s⁻¹ along armchair direction; and 246 cm²V⁻¹s⁻¹ along zigzag direction). The high mobility of δ -Cu₂S bilayer also stems from the small carrier effective masses ($\sim 0.16 m_0$), small deformation potential constant (~ 3.03 eV), and large elastic modulus (~ 95 J•m⁻²). The hole mobility of δ -Cu₂S bilayer (up to 2107 cm²V⁻¹s⁻¹) is notably higher than that of monolayer counterpart, as well as than that (79 \sim 109 cm²V⁻¹s⁻¹) of β -Cu₂S bilayer. Therefore, δ -Cu₂S monolayer and bilayer possess more prominent carrier transport

properties than β -Cu₂S bilayer, making layered δ -Cu₂S a very promising candidate for future applications in electronic devices.

Conclusions

We have predicted a new phase of Cu₂S monolayer (δ -Cu₂S) and explored its atomic structure, bonding character, structural, thermal and chemical stabilities, and electronic properties. Specifically, δ -Cu₂S sheets are energetically more favorable compared to the recently synthesized 2D β -Cu₂S sheets, and have excellent dynamical and thermal stabilities. Importantly, the dissociation and chemisorption of O₂ on δ -Cu₂S are kinetically hampered by relatively high activation energy of 1.98 eV, suggesting that δ -Cu₂S can better withstand oxidation in the ambient. δ -Cu₂S has a modest direct band gap of 1.26 eV, and ultrahigh electron mobility up to 6880 cm²V⁻¹s⁻¹. The large difference between electron and hole mobility can be valuable to the efficient separation of electrons and holes for solar conversion applications. Furthermore, δ -Cu₂S bilayer possesses lower formation energy and much higher carrier mobility (~5786 cm²V⁻¹s⁻¹) than β -Cu₂S bilayer. Given that the β -Cu₂S sheets have been recently synthesized in the laboratory, it is expected that δ -Cu₂S sheets can be fabricated in near future. In view of its combination of novel electronic properties and superior oxidation resistance, δ -Cu₂S sheets may play even more important role in future 2D electronic devices than β -Cu₂S sheets.

Computational Methods

First-principles calculations were performed by using the Vienna *ab initio* simulation package (VASP 5.4),⁵¹ with the plane-wave basis set with an energy cutoff of 500 eV, the projector augmented wave potentials (PAW),^{52, 53} and the generalized gradient approximation

parameterized by Perdew, Burke and Ernzerhof (GGA-PBE) for the exchange-correlation functional.⁵⁴ The convergence criteria for total energy and residual force on each atom were set to 10^{-7} eV and 0.01 eV/Å, respectively. For unit cell of 2D δ -Cu₂S system, the Brillouin zone was sampled with a Γ -centered $16 \times 16 \times 1$ Monkhorst-Pack⁵⁵ \mathbf{k} -points grid. Note that the standard GGA functional tends to underestimate the band gaps; thus a hybrid functional (HSE06)⁵⁶ was also used to compute the electronic band structures of δ -Cu₂S. The climbing-image nudged elastic band (CI-NEB) method⁵⁷ was employed to investigate the adsorption kinetics of O₂ molecule, and to determine the activation energy for chemisorption. To this end, a $3 \times 3 \times 1$ supercell that contains 18 S atoms and 36 Cu atoms were built. Five images were used to calculate the reaction path. The intermediate image of each CI-NEB simulation was relaxed until the perpendicular forces were less than 0.02 eV/Å. The DFT-D3 method⁵⁸ was used to take into account the long-range van der Waals (vdW) interactions in the O₂ adsorption and layered systems.

To examine the dynamical stability of δ -Cu₂S monolayer, phonon dispersion was computed using the Phonopy code based on the density functional perturbation theory (DFPT)⁵⁹ as incorporated with VASP. The Born-Oppenheimer molecular dynamics (BOMD) simulations with the PAW method and PBE functional were carried out to assess thermal stabilities of the predicted δ -Cu₂S. In the BOMD simulations, the initial configuration of δ -Cu₂S with $3 \times 3 \times 1$ supercell was annealed under several temperatures. Each BOMD simulation in NVT ensemble lasted for 10 ps with a time step of 1.0 fs, and the temperature was controlled by using the Nosé-Hoover method.⁵⁹

The particle-swarm optimization (PSO) method implemented in CALYPSO code^{60, 61} was employed to search for low-energy structures of 2D (Cu₂S)_{*n*} ($n = 1 - 4$) monolayer sheets. As an

unbiased global optimization method, the PSO algorithm has successfully predicted a variety of 2D structures with high stability.⁶²⁻⁶⁷ In our PSO search, both the population size and the number of generation were set to 30. The required structural relaxations were performed by using PBE functional, as implemented in VASP 5.4 code.⁵¹

Conflicts of interest

There are no conflicts to declare.

Acknowledgements

Y.G. and Q.W. contributed equally to this work. This work was supported by the National Natural Science Foundation of China (11574040, 21525311, 21373045, 21773027, 21403005, 21803002), the Fundamental Research Funds for the Central Universities of China (DUT16-LAB01, DUT17LAB19), the National Key Research and Development Program of China (No. 2017YFA0204800), and Jiangsu 333 project (BRA2016353). Y. G. is supported by China Scholarship Council (CSC, 201706060138). Q.W. is supported by CSC (201606090079) and the Scientific Research Foundation of Graduate School of Southeast University (YBJJ1720). X.C.Z. is supported by the National Science Foundation (NSF) through the Nebraska Materials Research Science and Engineering Center (MRSEC) (grant No. DMR-1420645). We acknowledge the computing resource from the Supercomputing Center of Dalian University of Technology, the University of Nebraska Holland Computing Center and National Supercomputing Center in Tianjin.

References

- 1 Y. Xie, L. Carbone, C. Nobile, V. Grillo, S. D'Agostino, F. Della Sala, C. Giannini, D. Altamura, C. Oelsner, C. Kryschi and P.D. Cozzoli, *ACS Nano*, 2013, **7**, 7352-7369.
- 2 J.M. Luther, P.K. Jain, T. Ewers and A.P. Alivisatos, *Nat. Mater.*, 2011, **10**, 361.
- 3 S.-W. Hsu, K. On and A.R. Tao, *J. Am. Chem. Soc.*, 2011, **133**, 19072-19075.
- 4 Y. Zhao, H. Pan, Y. Lou, X. Qiu, J. Zhu and C. Burda, *J. Am. Chem. Soc.*, 2009, **131**, 4253-4261.
- 5 H. Zheng, J.B. Rivest, T.A. Miller, B. Sadtler, A. Lindenberg, M.F. Toney, L.-W. Wang, C. Kisielowski and A.P. Alivisatos, *Science*, 2011, **333**, 206.
- 6 S. He, G.-S. Wang, C. Lu, J. Liu, B. Wen, H. Liu, L. Guo and M.-S. Cao, *J. Mater. Chem. A*, 2013, **1**, 4685-4692.
- 7 B. Zhao, G. Shao, B. Fan, W. Zhao, Y. Xie and R. Zhang, *J. Mater. Chem. A*, 2015, **3**, 10345-10352.
- 8 B. Li, L. Huang, G. Zhao, Z. Wei, H. Dong, W. Hu, L.-W. Wang and J. Li, *Adv. Mater.*, 2016, **28**, 8271-8276.
- 9 R. Cai, J. Chen, J. Zhu, C. Xu, W. Zhang, C. Zhang, W. Shi, H. Tan, D. Yang, H.H. Hng, T.M. Lim and Q. Yan, *J. Phys. Chem. C*, 2012, **116**, 12468-12474.
- 10 F. Han, W.-C. Li, D. Li and A.-H. Lu, *ChemElectroChem*, 2014, **1**, 733-740.
- 11 Y. Kim, K.Y. Park, D.M. Jang, Y.M. Song, H.S. Kim, Y.J. Cho, Y. Myung and J. Park, *J. Phys. Chem. C*, 2010, **114**, 22141-22146.
- 12 R.L.N. Chandrakanthi and M.A. Careem, *Thin Solid Films*, 2002, **417**, 51-56.
- 13 G. Liu, T. Schulmeyer, J. Brötz, A. Klein and W. Jaegermann, *Thin Solid Films*, 2003, **431-432**, 477-482.
- 14 M. Ashry and S.A. Fayek, *Renew. Energy*, 2001, **23**, 441-450.
- 15 L.-W. Wang, *Phys. Rev. Lett.*, 2012, **108**, 085703.
- 16 S.-H. Lee, Y. Jung and R. Agarwal, *Nat. Nanotechnol.*, 2007, **2**, 626.
- 17 M.H.R. Lankhorst, B.W.S.M.M. Ketelaars and R.A.M. Wolters, *Nat. Mater.*, 2005, **4**, 347.
- 18 K.S. Novoselov, A.K. Geim, S.V. Morozov, D. Jiang, Y. Zhang, S.V. Dubonos, I.V. Grigorieva and A.A. Firsov, *Science*, 2004, **306**, 666.
- 19 Y. Liu, N.O. Weiss, X. Duan, H.-C. Cheng, Y. Huang and X. Duan, *Nat. Rev. Mater.*, 2016, **1**, 16042.
- 20 M. Xu, T. Liang, M. Shi and H. Chen, *Chem. Rev.*, 2013, **113**, 3766-3798.
- 21 M. Li, J. Dai and X.C. Zeng, *Nanoscale*, 2015, **7**, 15385-15391.
- 22 Y. Hong, J. Zhang and X.C. Zeng, *Nanoscale*, 2018, **10**, 4301-4310.
- 23 L. Ma, M.-G. Ju, J. Dai and X.C. Zeng, *Nanoscale*, 2018, **10**, 11314-11319.
- 24 F.B. Romdhane, O. Cretu, L. Debbichi, O. Eriksson, S. Lebègue and F. Banhart, *Small*, 2015, **11**, 1253-1257.

- 25 S. Rauf, K. TaeWan, M. Jihun and K. Sang-Woo, *Nanotechnology*, 2017, **28**, 505601.
- 26 J.B. Rivest, L.-K. Fong, P.K. Jain, M.F. Toney and A.P. Alivisatos, *J. Phys. Chem. Lett.*, 2011, **2**, 2402-2406.
- 27 K. Anuar, Z. Zainal, M.Z. Hussein, N. Saravanan and I. Haslina, *Energy Mater. Sol. Cells*, 2002, **73**, 351-365.
- 28 C.-G. Andres, V. Leonardo, P. Elsa, O.I. Joshua, K.L. Narasimha-Acharya, I.B. Sofya, J.G. Dirk, B. Michele, A.S. Gary, J.V. Alvarez, W.Z. Henny, J.J. Palacios and S.J.v.d.Z. Herre, *2D Mater.*, 2014, **1**, 025001.
- 29 O.I. Joshua, A.S. Gary, S.J.v.d.Z. Herre and C.-G. Andres, *2D Mater.*, 2015, **2**, 011002.
- 30 A. Ziletti, A. Carvalho, D.K. Campbell, D.F. Coker and A.H. Castro Neto, *Phys. Rev. Lett.*, 2015, **114**, 046801.
- 31 Y. Guo, S. Zhou, Y. Bai and J. Zhao, *J. Chem. Phys.*, 2017, **147**, 104709.
- 32 Y. Guo, S. Zhou, Y. Bai and J. Zhao, *ACS Appl. Mater. Interfaces*, 2017, **9**, 12013-12020.
- 33 J.-S. Kim, Y. Liu, W. Zhu, S. Kim, D. Wu, L. Tao, A. Dodabalapur, K. Lai and D. Akinwande, *Sci. Rep.*, 2015, **5**, 8989.
- 34 A. Savin, R. Nesper, S. Wengert and T.F. Fässler, *Angew. Chem.-Int. Edit.*, 1997, **36**, 1808-1832.
- 35 A. Savin, O. Jepsen, J. Flad, O.K. Andersen, H. Preuss and H.G. von Schnering, *Angew. Chem.-Int. Edit.*, 1992, **31**, 187-188.
- 36 A.D. Becke and K.E. Edgecombe, *J. Chem. Phys.*, 1990, **92**, 5397-5403.
- 37 R.F.W. Bader, *Acc. Chem. Res*, 1985, **18**, 9-15.
- 38 J. Hernández-Trujillo and R.F.W. Bader, *J. Phys. Chem. A*, 2000, **104**, 1779-1794.
- 39 G. Gabriella, K. Jiří, F.-A. Felix and M. Angelos, *J Phys. Condens Mat.*, 2012, **24**, 424216.
- 40 Y. Cai, G. Zhang and Y.-W. Zhang, *Sci. Rep.*, 2014, **4**, 6677.
- 41 S. Kc, R.C. Longo, R.M. Wallace and K. Cho, *J. Appl. Phys.*, 2015, **117**, 135301.
- 42 J.G. Speight, *Lange's handbook of chemistry*, McGraw-Hill New York, 2005.
- 43 H.J. Conley, B. Wang, J.I. Ziegler, R.F. Haglund, Jr., S.T. Pantelides and K.I. Bolotin, *Nano Lett.*, 2013, **13**, 3626-3630.
- 44 A.R. Klots, A.K.M. Newaz, B. Wang, D. Prasai, H. Krzyzanowska, J. Lin, D. Caudel, N.J. Ghimire, J. Yan, B.L. Ivanov, K.A. Velizhanin, A. Burger, D.G. Mandrus, N.H. Tolk, S.T. Pantelides and K.I. Bolotin, *Sci. Rep.*, 2014, **4**, 6608.
- 45 G. Fiori and G. Iannaccone, *Proc. IEEE*, 2013, **101**, 1653-1669.
- 46 S. Bruzzone and G. Fiori, *Appl. Phys. Lett.*, 2011, **99**, 222108.
- 47 S. Takagi, A. Toriumi, M. Iwase and H. Tango, *IEEE Trans. Electron Devices*, 1994, **41**, 2357-2362.
- 48 J. Qiao, X. Kong, Z.-X. Hu, F. Yang and W. Ji, *Nat. Commun.*, 2014, **5**, 4475.

- 49 G. Yu, Z. Si, Z. Junfeng, B. Yizhen and Z. Jijun, *2D Mater.*, 2016, **3**, 025008.
- 50 W. Zhang, Z. Huang, W. Zhang and Y. Li, *Nano Res.*, 2014, **7**, 1731-1737.
- 51 G. Kresse and J. Furthmüller, *Phys. Rev. B*, 1996, **54**, 11169-11186.
- 52 G. Kresse and D. Joubert, *Phys. Rev. B*, 1999, **59**, 1758-1775.
- 53 P.E. Blöchl, *Phys. Rev. B*, 1994, **50**, 17953-17979.
- 54 J.P. Perdew, K. Burke and M. Ernzerhof, *Phys. Rev. Lett.*, 1996, **77**, 3865-3868.
- 55 H.J. Monkhorst and J.D. Pack, *Phys. Rev. B*, 1976, **13**, 5188-5192.
- 56 J. Heyd, G.E. Scuseria and M. Ernzerhof, *J. Phys. Chem. C*, 2003, **118**, 8207-8215.
- 57 G. Mills, H. Jónsson and G.K. Schenter, *Surf. Sci.*, 1995, **324**, 305-337.
- 58 L.A. Burns, Á.V. Mayagoitia, B.G. Sumpter and C.D. Sherrill, *J. Chem. Phys.*, 2011, **134**, 084107.
- 59 S. Baroni, S. de Gironcoli, A. Dal Corso and P. Giannozzi, *Rev. Mod. Phys.*, 2001, **73**, 515-562.
- 60 Y. Wang, M. Miao, J. Lv, L. Zhu, K. Yin, H. Liu and Y. Ma, *J. Phys. Chem. C*, 2012, **137**, 224108.
- 61 Y. Wang, J. Lv, L. Zhu and Y. Ma, *Phys. Rev. B*, 2010, **82**, 094116.
- 62 Q. Wu, W.W. Xu, B. Qu, L. Ma, X. Niu, J. Wang and X.C. Zeng, *Mater. Horizons*, 2017, **4**, 1085-1091.
- 63 Y. Ma, A. Kuc and T. Heine, *J. Am. Chem. Soc.*, 2017, **139**, 11694-11697.
- 64 Y. Li, Y. Liao and Z. Chen, *Angew. Chem.-Int. Edit.*, 2014, **53**, 7248-7252.
- 65 X. Wu, J. Dai, Y. Zhao, Z. Zhuo, J. Yang and X.C. Zeng, *ACS Nano*, 2012, **6**, 7443-7453.
- 66 X. Luo, J. Yang, H. Liu, X. Wu, Y. Wang, Y. Ma, S.-H. Wei, X. Gong and H. Xiang, *J. Am. Chem. Soc.*, 2011, **133**, 16285-16290.
- 67 F. Ma, Y. Jiao, G. Gao, Y. Gu, A. Bilic, Z. Chen and A. Du, *Nano Lett.*, 2016, **16**, 3022-3028.